J Mater Sci (2021) 56:18006–18018

Chemical routes to materials

One-pot synthesis of glucose-derived carbonaceous material with high hydrophilicity and adsorption capacity as bilirubin adsorbent

Xiaowei Li[1,3], Haiyang Zhang[1,2], Jing Dong[1], Shujuan Ma[1,2], and Junjie Ou[1,*]

[1] CAS Key Laboratory of Separation Science for Analytical Chemistry, Dalian Institute of Chemical Physics, Chinese Academy of Sciences (CAS), Dalian 116023, China
[2] Key Laboratory of Synthetic and Natural Function Molecule Chemistry of Ministry of Education, College of Chemistry and Materials Science, Northwest University, Xi'an 710069, China
[3] University of Chinese Academy of Sciences, Beijing 100049, China

Received: 2 June 2021
Accepted: 18 August 2021
Published online: 1 September 2021

© The Author(s), under exclusive licence to Springer Science+Business Media, LLC, part of Springer Nature 2021

ABSTRACT

A novel bilirubin adsorbent with high hydrophilicity was facilely synthesized via one-step hydrothermal carbonization reaction by using glucose and [3-(methacryloylamino)propyl]trimethylammonium chloride (MAPTAC) as precursors, in which sustainable carbohydrate could be converted into functionalized carbonaceous materials enriched with quaternary ammonium groups using an environmentally mild process. The properties of synthesized adsorbents were characterized by helium ion microscopy, static water contact angle measurement, FT-IR, elemental analysis and nitrogen adsorption/desorption measurement. The contact angle results indicated that these materials possessed very good hydrophilicity along with the lowest contact angle at 16.2°. Moreover, the hydrophilic adsorbent prepared by only one-step demonstrated good adsorption capacity toward bilirubin (141 mg/g) than commercialized activated carbon (70 mg/g) and low non-specific adsorption toward albumin (0.21%), which had great potential to be used in hemoperfusion. In addition, kinetic adsorption behaviors were conducted using pseudo-first-order and pseudo-second-order models. The regression results showed that the kinetic adsorption data were more accurately represented by pseudo-second-order model. The equilibrium adsorption data were analyzed using two widely applied isotherm models: Langmuir and Freundlich. The results revealed that Langmuir isotherm matched the experimental results well.

Handling Editor: Christopher Blanford.

Address correspondence to E-mail: junjieou@dicp.ac.cn

https://doi.org/10.1007/s10853-021-06456-2

GRAPHICAL ABSTRACT

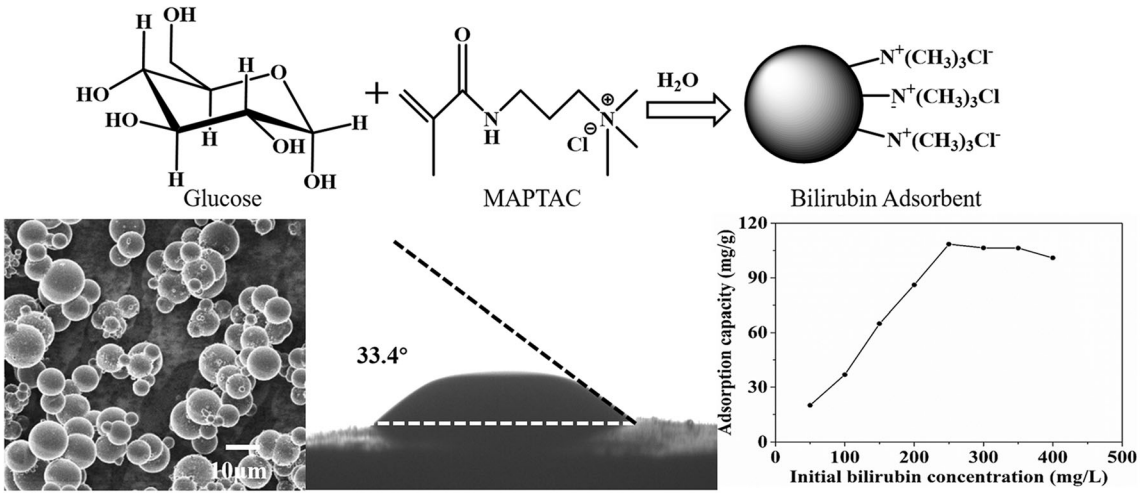

Introduction

As an index of liver function levels [1], bilirubin is a kind of lipophilic endotoxin generated from the degradation of hemoglobin. Usually, it is transported to the liver to form a water-soluble complex with glucuronic acid in the presence of bilirubin glucuronyl transferase and further excreted from the hepatocytes to the bile [2]. However, for patients with liver failure, hepatitis or other liver diseases, an excess amount of bilirubin accumulates in blood since the lack of liver detoxifying function, which is called hyperbilirubinemia. It can cause permanent damage to the brain and nervous systems, and even leading to death [3]. Accordingly, removal of bilirubin plays an important role in human health, and it is crucial to gain more chances and time for liver transplantation and regeneration of the damaged liver [4]. Several techniques have been used clinically, such as hemoperfusion, hemodialysis and molecular adsorbent recycling system (MARS). Of them, hemoperfusion seems to be the most promising treatment due to its ease of handling, lower cost and its prevention of blood damage [5], in which bilirubin was adsorbed through an extracorporeal unit incorporating an adsorbent system. The curative efficiency of hemoperfusion critically depends on the performance of adsorbents [6]. Consequently, the development of high efficient adsorbents is the focus in hemoperfusion research and development.

It has been found that bilirubin could be removed through electrostatic interaction, hydrogen bond interaction or hydrophobic interaction by adsorbents containing functional ligands like amino, carboxyl or hydroxyl groups [4]. In recent studies, a number of adsorbents have been specially designed for bilirubin removal, such as activated carbon [7, 8], ordered mesoporous carbon [9], ion-exchange resins [10], porous carbon [11], titania particles [5], metal–organic frameworks (MOFs) [12], porous aromatic frameworks (PAFs) [13] and multifunctional composite membrane [14]. Meanwhile, many modification methods have been used to improve the ability of adsorbents for removing bilirubin. However, there are still some disadvantages among aforementioned materials. For example, activated carbon is the most commonly used material with low price, but it has strong non-specific blood protein adsorption, which would significantly reduce their adsorption ability toward bilirubin and result in serious clinical side effects [15, 16]. For the modified materials, the modification procedure is usually complicated and time-consuming. Moreover, current coating materials could not fully eliminate the side effects in hemoperfusion applications yet. The development of novel bilirubin adsorbents with better performance and low cost is still urgently desired.

Hydrothermal carbon (HTC) has attracted great attentions in a wide variety of applications, such as catalyst [17–20], adsorbents [21–26] and electrode materials [27]. Compared with other frequently used base materials like silica materials, carbon materials are difficult to be functionalized. Normally, carbonization process requires harsh and rather expensive processing conditions such as high temperatures [28, 29], chemical vapor deposition [30, 31] or arc discharge [32]. Fortunately, a cheap, easy and environmental route to prepare carbonaceous materials was presented by Titirici and co-workers [21]. They described the synthesis of a new type of carboxylate-rich carbonaceous material via one-step hydrothermal carbonization of glucose in the presence of acrylic acid monomer. The synthesized materials proved to be feasible to remove heavy metals from aqueous solutions. Similarly, Su and co-workers [18] prepared the same carboxylate-rich carbonaceous material as a carbocatalyst in the Beckmann rearrangement of cyclohexanone oxime, which exhibited superior performance compared with conventional solid acid. In the hydrothermal carbonization reaction, ubiquitously available and renewable biomass such as glucose, sucrose and cellulose could be converted into carbon based materials by one step, and the co-monomers were added to provide the functionality. It offered us a hint to fabricate bilirubin adsorbents.

In this study, we prepared a kind of carbonaceous material enriched with quaternary ammonium groups using hydrothermal carbonization of glucose in the presence of [3-(methacryloylamino)propyl] trimethylammonium chloride (MAPTAC). The physical and chemical properties of the resulting carbonaceous materials were characterized with helium ion microscopy (HIM), static water contact angle measurement, FT-IR, elemental analysis and nitrogen adsorption/desorption measurement. The resulting carbonaceous materials were applied for the removal of bilirubin. In order to explain the adsorption behaviors, two adsorption kinetic models and two adsorption isotherm models toward bilirubin were evaluated. At the same time, the non-specific adsorption to albumin was investigated.

Experimental section

Materials

Glucose and bilirubin (98%) were obtained from Aladdin (Shanghai, China). Sodium chloride (NaCl), potassium chloride (KCl), sodium phosphate dibasic (Na_2HPO_4), potassium phosphate monobasic (KH_2PO_4) and MAPTAC solution (50%) were purchased from Sigma (St Louis, MO, USA). Ethanol (analytical grade) was from Tianjin Kermel Chemical Plant (Tianjin, China). Albumin from bovine serum (BSA) was from Roche (Shanghai, China). Enhanced BCA Protein Assay Kit (P0009) was from Beyotime (Shanghai, China). The water used in all experiments was doubly distilled and purified by Milli-Q system (Millipore Inc., Milford, MA, USA).

Synthesis of quaternary ammonium-rich carbonaceous materials via hydrothermal approach

To obtain functional hydrothermal materials with a high degree of quaternary ammonium groups, MAPTAC, a monomer containing quaternary ammonium group, was added into glucose solution. The mixture was transferred into a Teflon inlet in an autoclave and treated in an oven at 180 °C for 6 h. And the obtained carbonaceous materials were then washed with water and ethanol. Finally, the materials were dried under vacuum at 60 °C overnight prior to use. The synthesized materials were denoted as G_xM_y, where x and y represent the weight percentage of glucose and MAPTAC in the initial solution, respectively. In addition, a controlled sample, named as G_{10}, was prepared without adding MAPTAC. The synthesis process is shown in Fig. 1.

Characterization

For specific surface area analysis, the resulting materials were degassed at 120 °C over 6 h. Then, N_2 adsorption/desorption experiments were carried out at 77 K using ASAP 2460 Physisorption Analyzer (Micromeritics, USA). Helium ion microscopy (ORION NANOFAB, Germany) was used for morphology observation. Elemental analysis was obtained through an FLASH EA 1112 Elemental Analyzer (Thermo, USA). Water contact angles were measured on a DSA 100 machine (KRUSS, Hamburg,

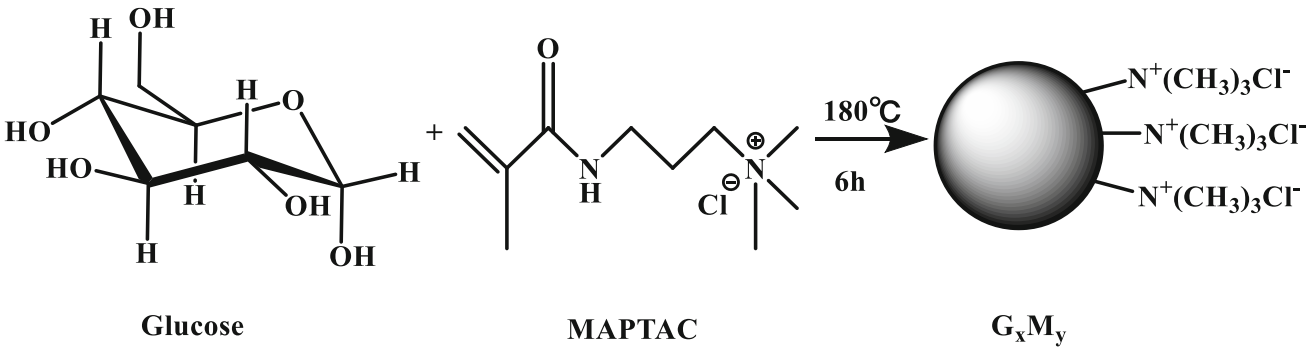

Figure 1 Schematic diagram of the synthesis process of G_xM_y.

Germany) with 5 μL of water drop after the obtained powders were prepared into tablets under 5 MPa. FT-IR spectra were obtained on a TENSOR 27 spectrometer with KBr pellets containing carbonaceous sample (1 wt%, Bruker Optics, Germany). Absorbance data of bilirubin in PBS (pH = 7.4) were tested on Synergy H1 microplate reader (BioTek, USA).

Ion-exchange capacity (IEC)

The ion-exchange capacities of samples were determined by Mohr titration. The 50 mg samples were immersed in 25 mL 0.5 M KNO_3 for 2 days to fully leach out all free Cl^-. The 5 ml supernatant were extracted after centrifugation and titrated with 0.01 M $AgNO_3$ using K_2CrO_4 as the indicator. The color changes from yellow to reddish brown determined the end point of the titration. The titration was repeated 3 additional times for each sample. The IEC of the samples was calculated using the following equation:

$$IEC = V_{AgNO3}C_{AgNO3}/m \quad (1)$$

where IEC (mmol/g) is the ion-exchange capacity; V_{AgNO3} (mL) and C_{AgNO3} (mmol/mL) are the volume and concentration of $AgNO_3$, respectively; m (g) is the weight of the adsorbent.

Adsorption of bilirubin

In the bilirubin adsorption experiments, 5 mg carbonaceous materials were added into a brown centrifuge tube containing 4 mL PBS of bilirubin under shaking at 200 rpm, 37 °C. The concentration of bilirubin was measured by microplate reader at a wavelength of 438 nm. In the kinetic experiments, the initial concentration of bilirubin was fixed at 200 mg/L, and the equilibrium concentration of bilirubin was measured at different time intervals. For the measurement of bilirubin adsorption isotherm experiments, the adsorption time was fixed at 1 h, and the initial concentration of bilirubin was changed. It is worth noting that all the adsorption experiments were repeated three times and carried out in a dark room due to the instability of bilirubin in visible light. The adsorption capacity was calculated by the following equation:

$$Q_e = V(C_0 - C_e)/m \quad (2)$$

where Q_e (mg/g) is the equilibrium adsorption capacity; C_0 (mg/L) and C_e (mg/L) are the initial and equilibrium concentrations of bilirubin, respectively; V (mL) is the volume of bilirubin PBS and m (mg) is the weight of the added adsorbent.

Adsorption of bilirubin in BSA solution

Similarly, to evaluate the adsorption performance toward bilirubin in the BSA solution, 5 mg carbonaceous materials were added to 4 mL bilirubin/BSA solution (pH: 7.4; bilirubin concentration: 200 mg/L; BSA concentration: 50 mg/mL), followed by shaking at 37 °C and 200 rpm. After shaking for 1 h, the supernatant absorbance at 452 nm was measured to determine the residual bilirubin concentration. All experiments were conducted under a dark environment and in triplicate.

Results and discussion

Synthesis and characterization

In order to obtain hydrothermal carbonaceous materials with a high degree of quaternary ammonium groups, glucose was used as carbon source, and

MAPTAC was added as a co-monomer. Different mass ratios of glucose and MAPTAC were employed. The reaction mixtures were hydrothermally treated at 180 °C for 6 h. During the hydrothermal carbonization reaction [33–35], furfural and furfural derivatives produced as intermediates from the dehydration of glucose. Then, a series of cycloadditions and condensation reactions took place in the intermediates [36, 37]. Lastly, the intermediates which contain the furan unit as the main repeating motif were involved in Diels–Alder type cycloaddition in the presence of dienophiles like MAPTAC in this work. As a result, hydrophilic carbonaceous microspheres with quaternary ammonium groups on the surface formed. The obtained carbonaceous samples were labeled according to the concentrations of glucose (quoted as G) and MAPTAC monomer (quoted as M) added into the initial reaction mixture. For instance, $G_{10}M_1$ means that glucose and MAPTAC account for 10 wt% and 1 wt% in the initial mixture, respectively. The carbonaceous material obtained from 10 wt% glucose solution without any MAPTAC monomer was called G_{10}.

Effects of initial concentration of monomers on morphology and hydrophilicity of carbonaceous materials

The concentrations of glucose and MAPTAC played vitally important roles in the formation of carbonaceous materials. A series of carbonaceous materials were fabricated with various concentrations of glucose and MAPTAC. As shown in Fig. 2, HIM images showed that the carbonaceous material prepared by sole precursor (G_{10}) was monodispersed microspheres with the size of around 200 nm. As for $G_{10}M_1$, corresponding to the initial concentrations of glucose and MAPTAC were 10 wt% and 1 wt% respectively, polydispersed carbon spheres were formed, and their size ranged in 1–10 μm. However, the carbonaceous materials became amorphous with an increase of the concentrations of glucose and MAPTAC ($G_{10}M_5$, $G_{10}M_{10}$, $G_{10}M_{20}$, $G_{20}M_{10}$ and $G_{20}M_{20}$), which might be due to the aggregation of the particles.

The porosities of the hydrothermal carbonaceous materials were determined by nitrogen adsorption–desorption measurement. Brunauer–Emmett–Teller

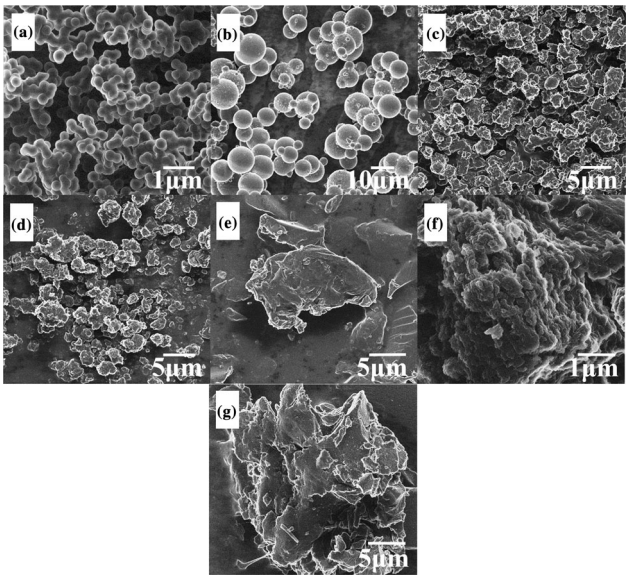

Figure 2 HIM images of **a** G_{10}, **b** $G_{10}M_1$, **c** $G_{10}M_5$, **d** $G_{10}M_{10}$, **e** $G_{10}M_{20}$, **f** $G_{20}M_{10}$ and **g** $G_{20}M_{20}$.

(BET) specific surface areas (Table 1) of $G_{10}M_1$, $G_{10}M_5$, $G_{10}M_{10}$, $G_{10}M_{20}$, $G_{20}M_{10}$ and $G_{20}M_{20}$ were 2.4, 53, 65, 0.71, 29 and 2.1 m^2/g, respectively. The above low specific surface areas are common for hydrothermal carbons [21]. In addition, it could be observed that the specific surface area increased first and then decreased with an increase of the concentration of MAPTAC while the concentration of glucose was fixed at 10 wt%. Among them, $G_{10}M_{10}$ exhibited the biggest specific surface area of 65 m^2/g. However, compared with $G_{10}M_{10}$, further increase of initial concentration of glucose could not improve the specific surface area of $G_{20}M_{10}$.

To evaluate the hydrophilicity of the resulting materials, static water contact angles of G_xM_y were investigated. As shown in Fig. 3, water contact angles of $G_{10}M_1$, $G_{10}M_5$, $G_{10}M_{10}$, $G_{10}M_{20}$, $G_{20}M_{10}$ and $G_{20}M_{20}$ were 33.4°, 22.5°, 24.8°, 23.5°, 20.4° and 16.2°, respectively. It could be concluded that G_xM_y possessed strongly hydrophilic with all water contact angles lower than 34°. Overall, the hydrophilicity of G_xM_y increased with the increase of initial concentration of either glucose or MAPTAC, which would be attributed to more hydrophilic groups-hydroxyl group and hydrophilic functional groups-quaternary ammonium group on the surface of resulting carbonaceous materials.

Table 1 Specific surface area, bilirubin adsorption capacity and relative standard deviation of adsorption capacity on G_xM_y

Sample	G_{10}	$G_{10}M_1$	$G_{10}M_5$	$G_{10}M_{10}$	$G_{10}M_{20}$	$G_{20}M_{10}$	$G_{20}M_{20}$
Sa (m^2/g)	\	2.4	53	65	0.71	29	2.1
Adsorption capacity (mg/g)	8.38	71.3	84.1	96.4	98.1	135	141
RSD (%)	0.716	5.05	8.69	6.47	11.51	5.45	8.83

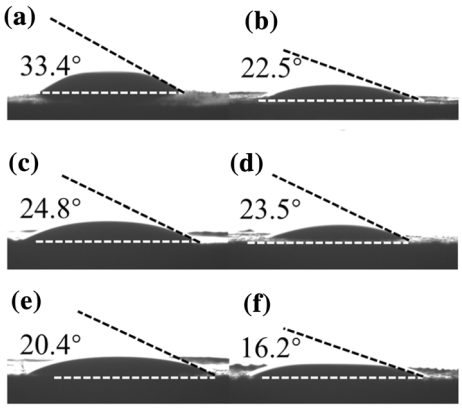

Figure 3 Water contact angle of **a** $G_{10}M_1$, **b** $G_{10}M_5$, **c** $G_{10}M_{10}$, **d** $G_{10}M_{20}$, **e** $G_{20}M_{10}$ and **f** $G_{20}M_{20}$.

FT-IR, elemental analysis and ion-exchange capacities of carbonaceous materials

The monomers and resulting materials were also analyzed by FT-IR (Fig. 4). Comparing with FT-IR spectra of two monomers, we could see the bands at 1700 cm^{-1} and 1620 cm^{-1} in $G_{10}M_1$ and $G_{10}M_{10}$, which could be attributed to C=O and C=C stretching vibrations, respectively. These results support the concept of aromatization of glucose during hydrothermal treatment [38]. In addition, the peak at 2900–3000 cm^{-1} and 1380 cm^{-1} in MAPTAC, $G_{10}M_1$ and $G_{10}M_{10}$ corresponds to the C–H stretching vibration and bending vibration in $–CH_3$, which was an important evidence for the existence of $–N^+(CH_3)_3$. This also proved the successful introduction of MAPTAC. However, the area of the most characteristic information of N–H was overlapped with the signals from O–H in the range of 3300–3400 cm^{-1}.

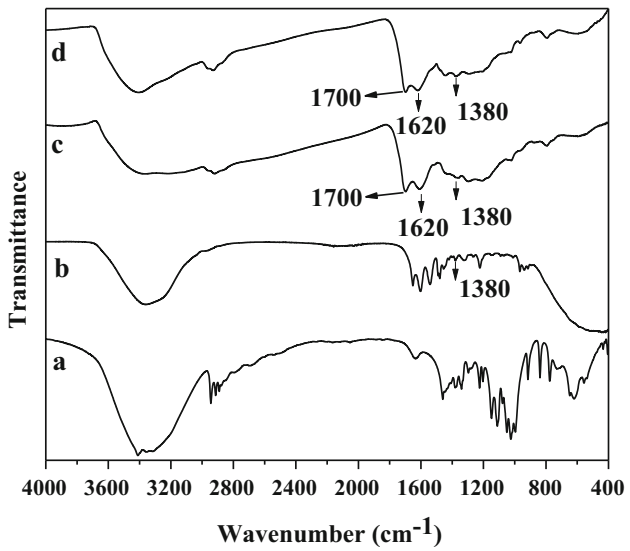

Figure 4 FT-IR spectra of **a** Glucose, **b** 50 wt% MAPTAC, **c** $G_{10}M_1$ and **d** $G_{10}M_{10}$.

The elemental analysis results are shown in Table 2. The content of nitrogen element in G_{10} was lower than the detection limit of instrument, indicating that there was no nitrogen element before grafting. After adding MAPTAC to the initial solution, the contents of nitrogen element in $G_{10}M_1$, $G_{10}M_5$, $G_{10}M_{10}$ and $G_{20}M_{20}$ were 0.56%, 1.70%, 2.80% and 2.83%, respectively. A conclusion could be drawn that the contents of nitrogen element increased as the mass ratio of MAPTAC to glucose increased in G_xM_y, indicating the successful introduction of MAPTAC in the carbonaceous materials.

Mohr titrations were employed to measure the IEC of the adsorbents. The results revealed that the IEC of $G_{10}M_1$ and $G_{10}M_{10}$ were 0.3 and 0.5 mmol/g, respectively, which increases with increased content of nitrogen element and correlates to a higher hydrophilicity. The results of Mohr titration were in good agreement with that of water contact angle measurement and elemental analysis, suggesting the successfully graft of MAPTAC into the surface of adsorbents, too.

Table 2 The results of elemental analysis of G_{10} and G_xM_y

Sample	C%	H%	N%
G_{10}	67.70	4.30	< 0.30
$G_{10}M_1$	68.14	4.74	0.56
$G_{10}M_5$	67.45	5.27	1.70
$G_{10}M_{10}$	66.38	5.64	2.80
$G_{20}M_{20}$	62.38	5.76	2.83

Application of carbonaceous materials for adsorption of bilirubin

Adsorption of bilirubin by different carbonaceous materials

Due to the existence of positively charged quaternary ammonium groups on the surface of carbonaceous materials, G_xM_y can be used to adsorb endogenous toxin bilirubin containing two carboxylate anions in a normal blood pH environment (about 7.4). In order to seek the optimal mass ratio of the adsorbents, various materials prepared by different mass ratios of precursors were applied in the adsorption experiments of bilirubin at the same adsorption condition. As shown in Table 1, the adsorption capacity of $G_{10}M_1$, $G_{10}M_5$, $G_{10}M_{10}$, $G_{10}M_{20}$, $G_{10}M_{20}$ and $G_{20}M_{20}$ was 71.3, 84.1, 96.4, 98.1, 135 and 141 mg/g, respectively. The materials with higher quaternary ammonium group contents reached a higher adsorption capacity. However, compared with $G_{10}M_{10}$, the adsorption capacity of $G_{10}M_{20}$ did not increase significantly when the mass ratio of MAPTAC to glucose further increased. And $G_{20}M_{20}$ exhibited the highest adsorption capacity of 141 mg/g in this work. For comparison, the adsorption capacity of G_{10} was also tested and found to be 8.38 mg/g, which was much lower than that of quaternary ammonium functionalized materials and confirmed the key role of quaternary ammonium groups in adsorption. Comparing with other reported bilirubin adsorbents (Table 3), we can find that the adsorption capacity of $G_{20}M_{20}$ was remarkably higher than commonly used clinical activated carbon (70 mg/g) [11] and some bilirubin adsorbents like titania films, resins and imprinted polymers [4, 40, 42–44]. Although the adsorption capacity of $G_{20}M_{20}$ was not as high as other materials with high specific surface areas like CMK-3 and HMCSs, the preparation process of adsorbent in this work was simpler [11].

Adsorption kinetics of bilirubin

Figure 5a shows the adsorption kinetic curves of bilirubin on G_xM_y. It could be observed that the adsorption capacity increased rather quickly at the initial stage and reached a plateau after 1 h. In addition, two general kinetic models including pseudo-first-order equation (shown in Fig. 5b) and pseudo-second-order equation (shown in Fig. 5c) were used to analyze the adsorption behavior of bilirubin on G_xM_y. Considering the morphology and specific surface area, we chose $G_{10}M_1$ and $G_{10}M_{10}$ for this experiment. Two equations could be represented as the following forms [45, 46]:

$$\text{pseudo-first-order: } \ln(Q_e - Q_t) = \ln(Q_{1cal}) - k_1 t \quad (3)$$

$$\text{pseudo-second-order: } t/Q_t = 1/\left(k_2 Q_{2cal}^2\right) + t/Q_{2cal} \quad (4)$$

where Q_e (mg/g) and Q_t (mg/g) are the adsorption capacity for bilirubin at equilibrium time and time t (min), respectively; Q_{1cal} (mg/g) and Q_{2cal} (mg/g) are the adsorption capacity calculated by pseudo-first-order kinetic model and pseudo-second-order kinetic model; $k_1$and k_2 are the rate constant of pseudo-first-order adsorption and pseudo-second-order adsorption.

In detail, we can judge from the correlation coefficient (r_1^2 and r_2^2) and the adsorption capacity calculated by two models (Q_{1cal} and Q_{2cal}) whether the

Table 3 Comparison of adsorption capacities for bilirubin of various reported adsorbents

No	Bilirubin adsorbent	Adsorption capacity (mg/g)	References
1	Activated carbon	70	[11]
2	CMK-3	198	[11]
3	HMCSs	304	[11]
4	$CS/GO_{10\%}$	178.25	[39]
5	Dye affinity microporous hollow fiber	48.9	[40]
6	PDA@L-lys	11.6	[41]
7	Anion exchange resin	4–80	[4]
8	Ch/CNT/Lys microsphere	107.2	[4]
9	Nanocrystalline titania film	17.08	[42]
10	Bilirubin imprinted poly(4-Vpy-co-DVB) film	62.0	[43]
11	BR-MIP cryogel	3.6	[44]
12	$G_{20}M_{20}$	141	This work

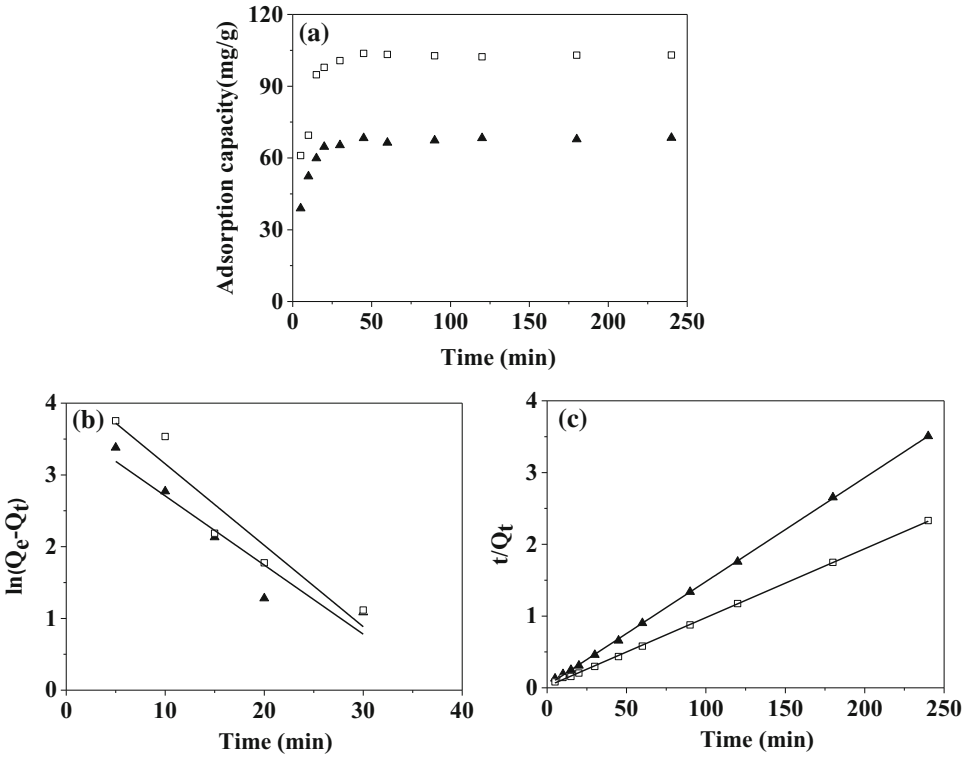

Figure 5 **a** The adsorption kinetic curves of bilirubin on $G_{10}M_1$ (▲) and $G_{10}M_{10}$ (□). Kinetic data of bilirubin adsorption on $G_{10}M_1$ (▲) and $G_{10}M_{10}$ (□) evaluated using **b** pseudo-first-order model and **c** pseudo-second-order model. Initial bilirubin concentration, 200 mg/L; temperature, 37 °C; medium, phosphate buffer (pH = 7.4).

adsorption behavior fits the kinetic model or not. As shown in Table 4, in pseudo-first-order model, the values of Q_{1cal} were 39.2 and 72.8 mg/g for $G_{10}M_1$ and $G_{10}M_{10}$, respectively, and the values of correlation coefficients (r_1^2) were about 0.9059 and 0.9194 for $G_{10}M_1$ and $G_{10}M_{10}$, respectively. Besides, the values of Q_{2cal} were 69.0 and 104 mg/g for $G_{10}M_1$ and $G_{10}M_{10}$, and the values of correlation coefficients (r_2^2) were about 0.9998 and 0.9997 for $G_{10}M_1$ and $G_{10}M_{10}$ in pseudo-second-order model. Moreover, the experimental Q_e were about 68.3 and 103 mg/g for $G_{10}M_1$ and $G_{10}M_{10}$, respectively. It was obvious that the adsorption capacity obtained from pseudo-second-order model (Q_{2cal}) was more consistent with the experimental data (Q_e), and the correlation coefficient in pseudo-second-order model (r_2^2) was higher and closer to 1. These results indicated that the bilirubin adsorption process on the G_xM_y fitted pseudo-second-order model very well. It also could be concluded that chemical interaction played a dominant role in the adsorption process [47], which was in accordance with the ionic bonding produced by electrostatic interaction between $-N^+(CH_3)_3$ in G_xM_y and $-COO^-$ in bilirubin.

Adsorption isotherm of bilirubin

The adsorption isotherm is usually used to study how the adsorbed molecules interact with the adsorbent, which is of great significance. Similarly, $G_{10}M_1$ and $G_{10}M_{10}$ were chosen to explain the effect of initial bilirubin concentration on the adsorption behavior. As indicated in Fig. 6a, the adsorption capacity increased with an increase of initial

Table 4 Kinetic parameters in pseudo-first-order and pseudo-second-order models of bilirubin on two materials

Sample	Experimental Q_e (mg/g)	Pseudo-first-order			Pseudo-second-order		
		k_1 (min^{-1})	Q_{1cal} (mg/g)	r_1^2	k_2 (g/mg·min)	Q_{2cal} (mg/g)	r_2^2
$G_{10}M_1$	68.3	0.0963	39.2	0.9059	0.006	69.0	0.9998
$G_{10}M_{10}$	103	0.1134	72.8	0.9194	0.005	104	0.9997

concentration of bilirubin, but remained unchanged after reaching a certain value in spite of further increasing initial concentration of bilirubin. In addition, we used Langmuir and Freundlich adsorption isotherms to investigate the adsorption process. Langmuir model assumes that there is no interaction between the adsorbed molecules and every adsorption site has the same adsorptive ability. In addition, the adsorption in Langmuir model is localized in a monolayer, while Freundlich model is applied to describe heterogeneous systems. Two equations could be expressed as the following forms [48, 49]:

$$\text{Langmuir isotherm: } C_e/Q_e = 1/(Q_m K_L) + C_e/Q_m \quad (5)$$

$$\text{Freundlich isotherm: } \lg(Q_e) = \lg(K_F) + (1/n)\lg(C_e) \quad (6)$$

where C_e (mg/L) is the equilibrium concentration of bilirubin in PBS; Q_e (mg/g) is the equilibrium adsorption capacity for bilirubin; Q_m (mg/g) is the maximum adsorption capacity; K_L (L/mg) is the Langmuir adsorption constant related to the energy of adsorption; K_F (mg/g) and $1/n$ are the Freundlich constants, indicating the capacity and intensity of adsorption, respectively.

The application of Langmuir adsorption isotherm and Freundlich adsorption isotherm for two chosen materials ($G_{10}M_1$ and $G_{10}M_{10}$) is shown in Fig. 6b, c, and the correlation coefficients for the Langmuir equation and Freundlich equation are listed in Table 5. As shown in Table 5, the correlation coefficients for the Langmuir equation (r_L^2) in $G_{10}M_1$ and $G_{10}M_{10}$ were both higher than 0.98, while the correlation coefficients for the Freundlich equation (r_F^2) were lower than the corresponding r_L^2. These data demonstrated that the adsorption of the resulting materials toward bilirubin fitted better with the Langmuir adsorption isotherm than the Freundlich isotherm, strongly indicating that the adsorption was a monolayer adsorption process.

Adsorption of BSA by different carbonaceous materials

Human serum albumin (HSA) is the most abundant protein in blood plasma. In practical applications, the high content of HSA greatly hinders the adsorption of bilirubin on adsorbent materials. Considering the lower price of BSA and the homology between HSA and BSA, the bilirubin adsorption experiments were conducted on the synthesized $G_{10}M_1$ and $G_{10}M_{10}$ with a high content of BSA (50 mg/mL) in the system to evaluate their performances. The results exhibited that the adsorption capacity of $G_{10}M_1$ and $G_{10}M_{10}$

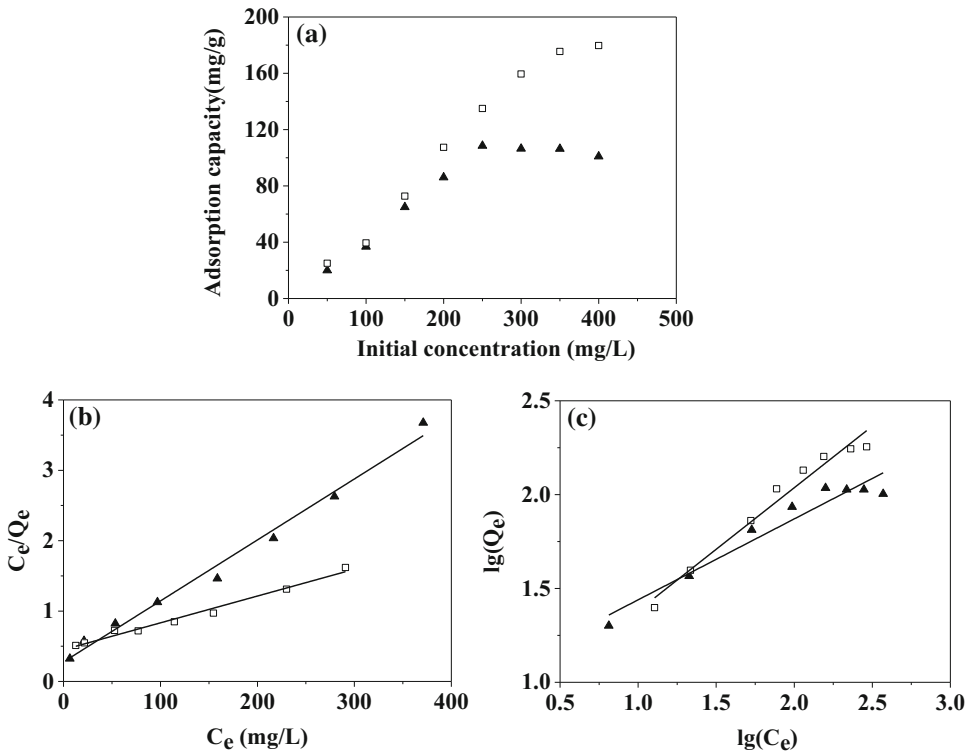

Figure 6 **a** The adsorption isotherm of bilirubin on $G_{10}M_1$ (▲) and $G_{10}M_{10}$ (□). Isotherm data of bilirubin adsorption on $G_{10}M_1$ (▲) and $G_{10}M_{10}$ (□) evaluated using **b** Langmuir isotherm model and **c** Freundlich isotherm model. Temperature, 37 °C; adsorption time, 1 h; medium, phosphate buffer (pH = 7.4).

Table 5 Adsorption isotherm parameters in Langmuir and Freundlich models of bilirubin on two materials

Sample	Langmuir isotherm model			Freundlich isotherm model		
	Q_m (mg/g)	K_L (L/mg)	r_L^2	n	K_F (mg/g)	r_F^2
$G_{10}M_1$	115	0.031	0.9880	2.32	10.20	0.9371
$G_{10}M_{10}$	263	0.008	0.9838	2.10	10.72	0.9712

toward bilirubin in BSA solution was 22.9 and 25.9 mg/g, respectively, which were higher than that of some previously reported materials like powdered activated carbon (8.0 mg/g in 40 mg/mL BSA) [50], CS/amino-WCNT (7.6 mg/g in 40 mg/mL BSA) [51] and PCB-H103 (20.8 mg/g in 40 mg/mL BSA) [52].

Adsorption of BSA by different carbonaceous materials

HSA serves as a transport and depot protein for numerous endogenous and exogenous compounds and is an important carrier and target molecule for drugs [53]. When the human plasma flows through the traditional hydrophobic bilirubin adsorbent, clinical activated carbon for instance, both albumin and bilirubin are adsorbed due to hydrophobic interaction between albumin and activated carbon, which could cause serious hypoproteinemia and will damage patient [11]. Therefore, it is of great importance to lower adsorption capacity toward albumin as a bilirubin adsorbent. Since the normal value of albumin concentration in human blood is 40–55 mg/mL, the initial concentration of BSA in the system was fixed at 50 mg/mL. During the test, 5 mg $G_{10}M_1$ or $G_{10}M_{10}$ were added into a centrifuge tube containing 4 mL PBS of BSA under shaking at 200 rpm, 37 °C for 1 h. Then, the concentration of BSA was measured with Enhanced BCA Protein Assay Kit. In detail, the initial concentration of prepared albumin solution was measured to be 50.96 mg/mL, and the concentrations of adsorbed albumin solution by $G_{10}M_1$ and $G_{10}M_{10}$ were found to be 49.49 mg/mL and 50.83 mg/mL, respectively. It is clear that the albumin concentration only decreased by 2.4% and 0.21% after the adsorption by $G_{10}M_1$ and $G_{10}M_{10}$, which was both relatively low. In addition, we can see that $G_{10}M_{10}$ have a lower albumin adsorption capacity compared with $G_{10}M_1$, indicating that $G_{10}M_{10}$ was more hydrophilic than $G_{10}M_1$, which was consistent with the contact angle results. As a result, relatively lower non-specific adsorption toward albumin was a great advantage of hydrophilic carbonaceous materials as a bilirubin adsorbent.

Conclusion

In this study, quaternary ammonium-enriched hydrothermal carbonaceous materials with good hydrophilicity were successfully synthesized by hydrothermal carbonization. The prepared carbonaceous materials could be used as a bilirubin adsorbent in hemoperfusion for removal of bilirubin from patients with liver diseases. Compared with the complicated and tedious synthesis process of other traditional bilirubin adsorbents, the preparation of adsorbent in this work only needs one step. Besides, this work offers a green synthesis method of bilirubin adsorbent in which cheap and widely available biomass-glucose could be converted into functionalized and hydrophilic carbonaceous materials. The bilirubin adsorption process on the carbonaceous materials fitted pseudo-second-order model and Langmuir adsorption isotherm. Furthermore, the bilirubin adsorbent synthesized in this study showed higher adsorption capacity toward bilirubin and lower non-specific adsorption toward albumin than commercially available activated carbon, which has great potential in hemoperfusion.

Acknowledgements

Financial support is gratefully acknowledged from the National Natural Sciences Foundation of China (No. 21974137), the CAS-Weigao Research & Development Program ([2017]-009) and the Innovation Program of Science and Research from the Dalian Institute of Chemical Physics (DICPI202005) to J. Ou.

Declarations

Conflict of interest The authors declare no competing financial interest.

References

[1] Yamazaki K, Shinke K, Ogino T (2013) Selective adsorption of bilirubin against albumin to oxidized single-wall carbon nanohorns. Colloids Surf B Biointerfaces 112:103–107

[2] Chou S-K, Syu M-J (2009) Via zinc(II) protoporphyrin to the synthesis of poly(ZnPP-MAA-EGDMA) for the imprinting and selective binding of bilirubin. Biomaterials 30(7):1255–1262

[3] Viggiano D, de Pascale E, Marinelli G, Pluvio C (2018) A comparison among three different apheretic techniques for treatment of hyperbilirubinemia. J Artif Organs 21(1):110–116

[4] Wu S, Duan B, Zeng X, Lu A, Xu X, Wang Y et al (2017) Construction of blood compatible lysine-immobilized chitin/carbon nanotube microspheres and potential applications for blood purified therapy. J Mater Chem B 5(16):2952–2963

[5] Asano T, Tsuru K, Hayakawa S, Osaka A (2008) Bilirubin adsorption property of sol–gel-derived titania particles for blood purification therapy. Acta Biomater 4(4):1067–1072

[6] Tao G, Zhang L, Hua Z, Chen Y, Guo L, Zhang J et al (2014) Highly efficient adsorbents based on hierarchically macro/mesoporous carbon monoliths with strong hydrophobicity. Carbon 66:547–559

[7] Müller BR (2010) Effect of particle size and surface area on the adsorption of albumin-bonded bilirubin on activated carbon. Carbon 48(12):3607–3615

[8] Annesini MC, Di Carlo C, Piemonte V, Turchetti L (2008) Bilirubin and tryptophan adsorption in albumin-containing solutions: I. Equilibrium isotherms on activated carbon. Biochem Eng J 40(2):205–210

[9] Huang S, Zheng J, Zhang Y, Zheng J, Zhuang Z, Yang Q et al (2020) Polydopamine decorated ordered mesoporous carbon for efficient removal of bilirubin under albumin-rich conditions. J Mater Chem B 8(2):290–297

[10] Piemonte V, Turchetti L, Annesini MC (2009) Bilirubin removal from albumin-containing solutions: dynamic adsorption on anionic resin. Asia-Pac J Chem Eng 5(5):708–713

[11] Guo L, Zhang L, Zhang J, Zhou J, He Q, Zeng S et al (2009) Hollow mesoporous carbon spheres-an excellent bilirubin adsorbent. Chem Commun 40:6071–6073

[12] Li Q, Zhao W, Guo H, Yang J, Zhang J, Liu M et al (2020) Metal-organic framework traps with record-high bilirubin removal capacity for hemoperfusion therapy. ACS Appl Mater Interfaces 12(23):25546–25556

[13] Zhao R, Ma T, Cui F, Tian Y, Zhu G (2020) Porous aromatic framework with tailored binding sites and pore sizes as a high-performance hemoperfusion adsorbent for bilirubin removal. Adv Sci (Weinh) 7(23):2001899

[14] Liu J, Shu G, Lu X, Li K, Kong X, Zheng S et al (2020) Alginate/HSA double-sided functional PVDF multifunctional composite membrane for bilirubin removal. Sep Purif Technol 252:117295

[15] Mikhalovsky SV (2003) Emerging technologies in extracorporeal treatment: focus on adsorption. Perfusion 18(1_suppl):47–54

[16] Howell CA, Sandeman SR, Zheng Y, Mikhalovsky SV, Nikolaev VG, Sakhno LA et al (2016) New dextran coated activated carbons for medical use. Carbon 97:134–146

[17] Makowski P, Demir Cakan R, Antonietti M, Goettmann F, Titirici M-M (2008) Selective partial hydrogenation of hydroxy aromatic derivatives with palladium nanoparticles supported on hydrophilic carbon. Chem Commun 8:999–1001

[18] Wen G, Wang B, Wang C, Wang J, Tian Z, Schlögl R et al (2016) Hydrothermal carbon enriched with oxygenated groups from biomass glucose as an efficient carbocatalyst. Angew Chem Int Ed 56(2):600–604

[19] Guo H, Lian Y, Yan L, Qi X, Smith RL (2013) Cellulose-derived superparamagnetic carbonaceous solid acid catalyst for cellulose hydrolysis in an ionic liquid or aqueous reaction system. Green Chem 15(8):2167–2174

[20] Lu Y-M, Zhu H-Z, Li W-G, Hu B, Yu S-H (2013) Size-controllable palladium nanoparticles immobilized on carbon nanospheres for nitroaromatic hydrogenation. J Mater Chem A 1(11):3783–3788

[21] Demir-Cakan R, Baccile N, Antonietti M, Titirici M-M (2009) Carboxylate-rich carbonaceous materials via one-step hydrothermal carbonization of glucose in the presence of acrylic acid. Chem Mater 21(3):484–490

[22] Xiong Y, Wang C, Wang H, Yao Q, Fan B, Chen Y et al (2017) A 3D titanate aerogel with cellulose as the adsorption-aggregator for highly efficient water purification. J Mater Chem A 5(12):5813–5819

[23] Qi X, Li L, Tan T, Chen W, Smith RL (2013) Adsorption of 1-Butyl-3-methylimidazolium chloride ionic liquid by functional carbon microspheres from hydrothermal carbonization of cellulose. Environ Sci Technol 47(6):2792–2798

[24] Chang B, Guan D, Tian Y, Yang Z, Dong X (2013) Convenient synthesis of porous carbon nanospheres with tunable pore structure and excellent adsorption capacity. J Hazard Mater 262:256–264

[25] Zhao R, Wang Y, Li X, Sun B, Li Y, Ji H et al (2016) Surface activated hydrothermal carbon-coated electrospun PAN fiber membrane with enhanced adsorption properties for herbicide. ACS Sustain Chem Eng 4(5):2584–2592

[26] Li X, Zhang H, Zhang N, Ma S, Ou J, Ye M (2019) One-step preparation of zwitterionic-rich hydrophilic hydrothermal carbonaceous materials for enrichment of N-glycopeptides. ACS Sustain Chem Eng 7(13):11511–11520
[27] Hu YS, Demir-Cakan R, Titirici MM, Müller JO, Schlögl R, Antonietti M et al (2008) Superior storage performance of a Si@SiOx/C nanocomposite as anode material for lithium-ion batteries. Angew Chem Int Ed 47(9):1645–1649
[28] Li F, Cheng HM, Xing YT, Tan PH, Su G (2000) Purification of single-walled carbon nanotubes synthesized by the catalytic decomposition of hydrocarbons. Carbon 38(14):2041–2045
[29] Haihui Y, Nevin N, Yury G, Almila GY, Constantine MM (2004) Wall structure and surface chemistry of hydrothermal carbon nanofibres. Nanotechnology 15(1):232
[30] Eftekhari A, Jafarkhani P, Moztarzadeh F (2006) High-yield synthesis of carbon nanotubes using a water-soluble catalyst support in catalytic chemical vapor deposition. Carbon 44(7):1343–1345
[31] Kitayama H, Shimizu K, Ohba T (2017) Graphene-laminated architectures obtained by chemical vapor deposition: from graphene to graphite. Chem Phys Lett 687:303–306
[32] Berkmans J, Jagannatham M, Reddy R, Haridoss P (2015) Synthesis of thin bundled single walled carbon nanotubes and nanohorn hybrids by arc discharge technique in open air atmosphere. Diamond Relat Mater 55:12–15
[33] Hu B, Wang K, Wu L, Yu S-H, Antonietti M, Titirici M-M (2010) Engineering carbon materials from the hydrothermal carbonization process of biomass. Adv Mater 22(7):813–828
[34] Gandini A, Coelho D, Gomes M, Reis B, Silvestre A (2009) Materials from renewable resources based on furan monomers and furan chemistry: work in progress. J Mater Chem 19(45):8656–8664
[35] Gandini A (2010) Furans as offspring of sugars and polysaccharides and progenitors of a family of remarkable polymers: a review of recent progress. Polym Chem 1(3):245–251
[36] Thomas A, Kuhn P, Weber J, Titirici M-M, Antonietti M (2009) Porous polymers: enabling solutions for energy applications. Macromol Rapid Commun 30(4–5):221–236
[37] Sevilla M, Fuertes AB (2009) Chemical and structural properties of carbonaceous products obtained by hydrothermal carbonization of saccharides. Chem A Eur J 15(16):4195–4203
[38] Sun X, Li Y (2004) Colloidal carbon spheres and their core/shell structures with noble-metal nanoparticles. Angew Chem Int Ed 43(5):597–601
[39] Wu K, Liu X, Li Z, Jiao Y, Zhou C (2020) Fabrication of chitosan/graphene oxide composite aerogel microspheres with high bilirubin removal performance. Mater Sci Eng C Mater Biol Appl 106:110162
[40] Şenel S, Denizli F, Yavuz H, Denizli A (2002) Bilirubin removal from human plasma by dye affinity microporous hollow fibers. Sep Sci Technol 37(8):1989–2006
[41] Tong Y, Guo B, Zhang B, Hou X, Geng F, Tian M (2020) Efficient synthesis of hollow solid phase extraction adsorbent using L-lysine modified polydopamine as coating shell for the selective recognition of bilirubin. Microchem J 158:105175
[42] Yang Z, Si S, Fung Y (2007) Bilirubin adsorption on nanocrystalline titania films. Thin Solid Films 515(7):3344–3351
[43] Wu A-H, Syu M-J (2006) Synthesis of bilirubin imprinted polymer thin film for the continuous detection of bilirubin in an MIP/QCM/FIA system. Biosens Bioelectron 21(12):2345–2353
[44] Baydemir G, Bereli N, Andaç M, Say R, Galaev IY, Denizli A (2009) Bilirubin recognition via molecularly imprinted supermacroporous cryogels. Colloids Surf B 68(1):33–38
[45] Thanh LHV, Liu J-C (2014) Flotation separation of soluble and colloidal indium from aqueous solution. Ind Eng Chem Res 53(3):1242–1248
[46] Ho YS, McKay G (1999) Pseudo-second order model for sorption processes. Process Biochem 34(5):451–465
[47] Wang H, Hu X, Guo Y, Qiu C, Long S, Hao D et al (2018) Removal of copper ions by few-layered graphene oxide nanosheets from aqueous solutions: external influences and adsorption mechanisms. J Chem Technol Biotechnol 93(8):2447–2455
[48] Yao Y, Xu F, Chen M, Xu Z, Zhu Z (2010) Adsorption behavior of methylene blue on carbon nanotubes. Bioresour Technol 101(9):3040–3046
[49] Uzun L, Denizli A (2006) Bilirubin removal performance of immobilized albumin in a magnetically stabilized fluidized bed. J Biomater Sci Polym Ed 17(7):791–806
[50] Cai N, Li Q, Zhang J, Xu T, Zhao W, Yang J et al (2017) Antifouling zwitterionic hydrogel coating improves hemocompatibility of activated carbon hemoadsorbent. J Colloid Interface Sci 503:168–177
[51] Zong W, Chen J, Han W, Chen J, Wang Y, Wang W et al (2018) Preparation of chitosan/amino multiwalled carbon nanotubes nanocomposite beads for bilirubin adsorption in hemoperfusion. J Biomed Mater Res B Appl Biomater 106(1):96–103
[52] Li Q, Yang J, Cai N, Zhang J, Xu T, Zhao W et al (2019) Hemocompatible hemoadsorbent for effective removal of protein-bound toxin in serum. J Colloid Interface Sci 555:145–156

[53] Kragh-Hansen U, Chuang VTG, Otagiri M (2002) Practical aspects of the ligand-binding and enzymatic properties of human serum albumin. Biol Pharm Bull 25(6):695–704

Publisher's Note Springer Nature remains neutral with regard to jurisdictional claims in published maps and institutional affiliations.